ESC European Society of Cardiology

Cardiovascular Research (2023) **119**, 2697–2711
https://doi.org/10.1093/cvr/cvad138

PDE4D mediates impaired β-adrenergic receptor signalling in the sinoatrial node in mice with hypertensive heart disease

Tristan W. Dorey, Megan D. McRae, Darrell D. Belke, and Robert A. Rose *

Libin Cardiovascular Institute, Department of Cardiac Sciences, Department of Physiology and Pharmacology, Cumming School of Medicine, University of Calgary, 3280 Hospital Drive NW, Calgary, AB, T2N 4Z6, Canada

Received 17 December 2022; revised 6 June 2023; accepted 18 July 2023; online publish-ahead-of-print 29 August 2023

Time of primary review: 49 days

Aims

The sympathetic nervous system increases HR by activating β-adrenergic receptors (β-ARs) and increasing cAMP in sinoatrial node (SAN) myocytes while phosphodiesterases (PDEs) degrade cAMP. Chronotropic incompetence, the inability to regulate heart rate (HR) in response to sympathetic nervous system activation, is common in hypertensive heart disease; however, the basis for this is poorly understood. The objective of this study was to determine the mechanisms leading to chronotropic incompetence in mice with angiotensin II (AngII)-induced hypertensive heart disease.

Methods and results

C57BL/6 mice were infused with saline or AngII (2.5 mg/kg/day for 3 weeks) to induce hypertensive heart disease. HR and SAN function in response to the β-AR agonist isoproterenol (ISO) were studied *in vivo* using telemetry and electrocardiography, in isolated atrial preparations using optical mapping, in isolated SAN myocytes using patch-clamping, and using molecular biology. AngII-infused mice had smaller increases in HR in response to physical activity and during acute ISO injection. Optical mapping of the SAN in AngII-infused mice demonstrated impaired increases in conduction velocity and altered conduction patterns in response to ISO. Spontaneous AP firing responses to ISO in isolated SAN myocytes from AngII-infused mice were impaired due to smaller increases in diastolic depolarization (DD) slope, hyperpolarization-activated current (I_f), and L-type Ca^{2+} current ($I_{Ca,L}$). These changes were due to increased localization of PDE4D surrounding β_1- and β_2-ARs in the SAN, increased SAN PDE4 activity, and reduced cAMP generation in response to ISO. Knockdown of PDE4D using a virus-delivered shRNA or inhibition of PDE4 with rolipram normalized SAN sensitivity to β-AR stimulation in AngII-infused mice.

Conclusions

AngII-induced hypertensive heart disease results in impaired HR responses to β-AR stimulation due to up-regulation of PDE4D and reduced effects of cAMP on spontaneous AP firing in SAN myocytes.

* Corresponding author. Tel: 403 210 3922, E-mail: robert.rose@ucalgary.ca

Graphical Abstract

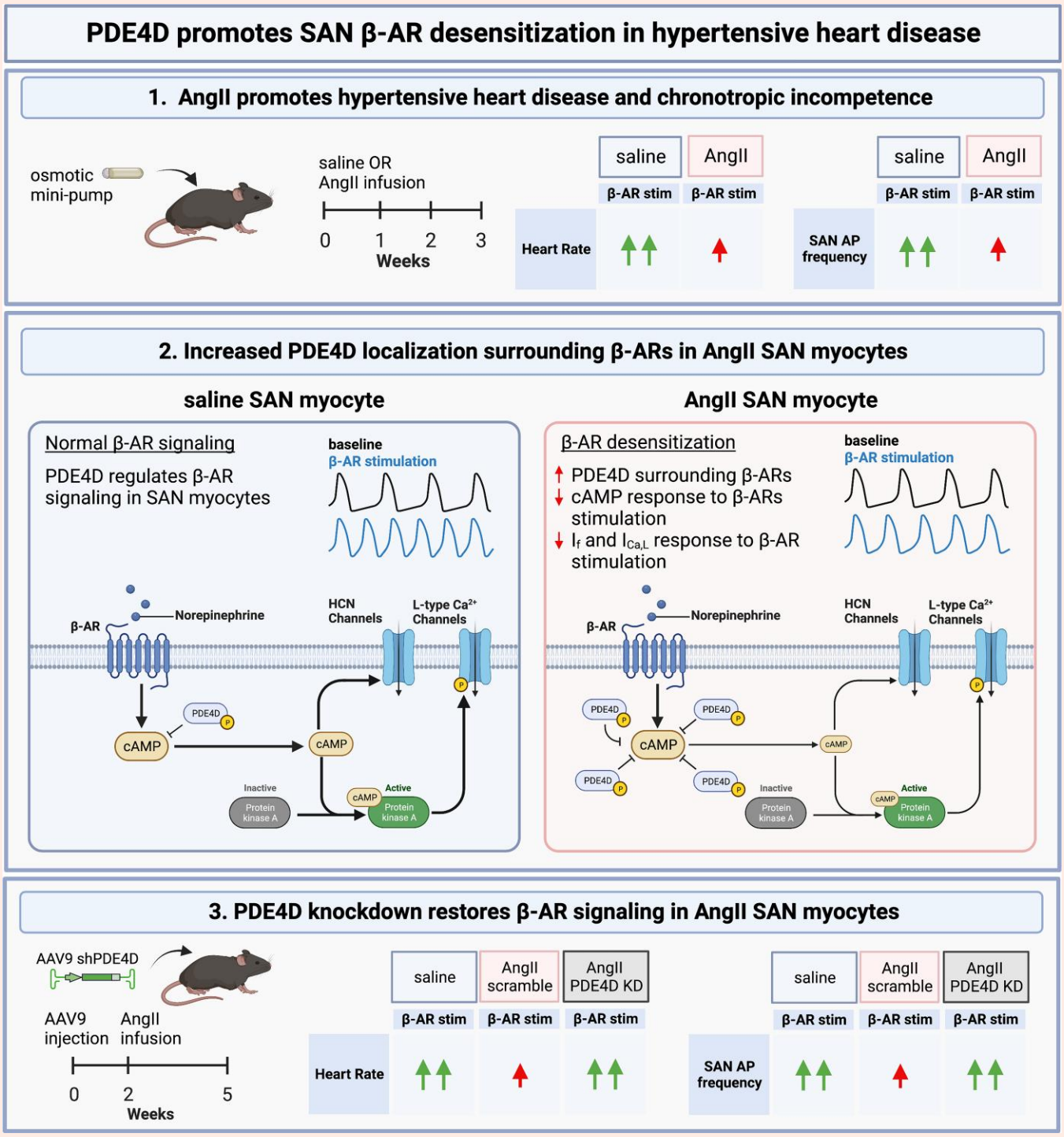

Keywords Chronotropic incompetence • Sinoatrial node • Heart rate • β-Adrenergic receptors • Phosphodiesterase • Ion channels

1. Introduction

Hypertension is the most common form of cardiovascular disease[1] and is the number one risk factor for the development of heart failure.[2,3] Hypertension increases myocardial work resulting in elevated sympathetic nervous system outflow to the heart as well as structural and electrical remodelling of the myocardium.[4] Heart rate (HR) is a critical regulator of cardiac performance that is controlled by the intrinsic properties of the sinoatrial node (SAN) and its modulation by the autonomic nervous system (ANS).[5,6] Impaired HR regulation in response to physical activity or

stress, denoted chronotropic incompetence, is common in the setting of hypertensive heart disease and heart failure and is associated with increased mortality.[7–9]

Increases in HR occur predominantly through sympathetic postganglionic release of norepinephrine onto SAN myocytes. Norepinephrine binds to β_1- and β_2-adrenergic receptors (ARs) on SAN myocytes, which activate adenylyl cyclase and increase cyclic adenosine monophosphate (cAMP) production.[5,6] A rise in intracellular cAMP elicits a positive shift in steady-state activation of the hyperpolarization-activated current (I_f) by direct binding of cAMP to hyperpolarization-activated cyclic nucleotide gated (HCN) channels. This results in larger inward current during the start of diastolic depolarization (DD) and an increase in SAN spontaneous action potential (AP) firing frequency.[6] Additionally, cAMP increases SAN myocyte AP firing via cAMP-mediated activation of protein kinase A (PKA) and subsequent increases in L-type Ca^{2+} current ($I_{Ca,L}$; carried by Cav1.2 and Cav1.3) and effects on sarcoplasmic reticulum (SR) Ca^{2+}-handling proteins that determine Ca^{2+} transient (CaT) morphology.[5,6,10] Membrane currents and SR Ca^{2+} handling represent a coupled system controlling diastolic depolarization in SAN myocytes.[10]

Phosphodiesterases (PDEs) are critical regulators of cAMP signalling in the SAN[11,12] and have been shown to blunt cardiac β-AR signalling.[13] PDE3 and PDE4 are major contributors to total PDE activity in the SAN and potently regulate SAN function.[11,12,14] The PDE4 family accounts for ~60% of total cardiac PDE activity in rodent hearts.[12,13,15] Furthermore, the PDE4D isoform predominantly regulates β-AR-induced cAMP signalling in the heart and is well conserved between rodent and human cardiomyocytes.[13,16–19]

Recent studies have demonstrated that chronotropic incompetence in the setting of human and animal models of hypertensive heart disease and heart failure result from SAN dysfunction, a blunting of maximum HR, as well as direct β-AR desensitization of the SAN.[20–22] Consistent with this, our lab has demonstrated that mice infused with the vasoconstrictor angiotensin II (AngII) have overt hypertensive heart disease, SAN dysfunction, and reduced responsiveness of the SAN to β-AR stimulation.[23,24] Despite these findings, the mechanisms responsible for β-AR desensitization of the SAN in hypertensive heart disease are still unknown. As such, the aim of the present study was to directly assess HR and SAN function in response to β-AR stimulation in mice with AngII-induced hypertensive heart disease. We show that AngII promotes progressive chronotropic incompetence due to impaired β-AR regulation of spontaneous AP firing in SAN myocytes and that PDE4D plays a major role in this process.

2. Methods

2.1 Experimental techniques

This study used male wildtype C57Bl/6 mice between the ages of 13 and 16 weeks. Mice were infused with saline or AngII (2.5 mg/kg/day) for 3 weeks using osmotic minipumps (Alzet, Cupertino, CA). Cardiac structure was assessed by echocardiography.[24,25] HR and SAN function were assessed using telemetry in awake and freely moving mice as well as electrocardiography in anaesthetized mice.[23,25] SAN function and conduction patterns were assessed using high-resolution optical mapping in isolated atrial preparations.[24–26] Spontaneous AP morphology and ionic currents (I_f, $I_{Ca,L}$) were investigated using patch-clamping in isolated SAN myocytes.[24,25] Ca^{2+} transient morphology was measured using Ca^{2+} imaging in isolated SAN myocytes. cAMP levels and PDE activity were assessed using commercially available kits.[25] SAN mRNA abundance and protein levels were investigated using qPCR and western blotting.[24,25] Co-localization of PDE4D and β-ARs was assessed using immunocytochemistry. In some cases, mice were injected retro-orbitally with a custom made adeno-associated virus stereotype-9 (AAV9; 1.5×10^{11} genomic copies/mouse) encoding an shRNA for murine PDE4D (or scrambled control) under the control of the U6 promoter (Vector Biolabs, Malvern, PA). Mice were used experimentally 5 weeks after virus injection. When combined with AngII infusion, AngII pumps were implanted two weeks after virus injection. For surgeries and tissue isolations, mice were anaesthetized using isoflurane (2%, inhalation). Mice were euthanized by cervical dislocation under isoflurane anaesthesia. Details for these approaches are available in the Data Supplement.

All experimental procedures were approved by the University of Calgary Animal Care and Use Committee and were in accordance with the guidelines of the Canadian Council on Animal Care and the NIH guide for the care and use of laboratory animals.

2.2 Statistics

All data are presented as means ± S.E.M. Statistical analysis was conducted using Prism version 9 (GraphPad Software). Normality of the data was assessed by Shapiro–Wilk test. Normally distributed data were analysed using Student's *t*-test, two-way analysis of variance (ANOVA) with a Holm-Sidak *post hoc* test, or two-way repeated measures ANOVA with a Holm-Sidak *post hoc* test as indicated in the figure legends. Non-parametric tests were used when data were not normally distributed. For cellular experiments, hierarchical statistical analyses were used to account for non-independent sampling (i.e. differences in the number of cells obtained from each animal). Statistical tests are reported in each figure legend, and differences are reported as $*P < 0.05$, $**P < 0.01$, $***P < 0.001$, or $****P < 0.0001$.

3. Results

3.1 Chronic AngII promotes chronotropic incompetence and β-AR desensitization *in vivo*

As expected,[24,27,28] three weeks of AngII infusion increased systolic and diastolic blood pressure (see Supplementary material online, *Figure S1A*) and resulted in cardiac hypertrophy as evident by increases in heart weight/tibia length (see Supplementary material online, *Figure S1B and C*). Echocardiography further demonstrates the occurrence of ventricular hypertrophy as indicated by increases in left ventricular anterior and posterior wall thickness, as well as reductions in left ventricular internal diameter, after 3 weeks of AngII infusion (see Supplementary material online, *Table S1*). Right and left atrial area was also increased after 3 weeks of AngII (see Supplementary material online, *Table S1*).

HR was monitored by telemetry in conscious mice during AngII (or saline) infusion (see Supplementary material online, *Figure S2*). Activity increased over three weeks of saline and AngII infusion with no differences between these groups (see Supplementary material online, *Figure S2A*). Conversely, increases in HR in association with increasing activity were reduced in AngII-infused mice (see Supplementary material online, *Figure S2B and C*). Intrinsic HR, measured during acute weekly injections of the ANS blockers atropine (10 mg/kg) and propranolol (10 mg/kg), also progressively declined during AngII infusion (see Supplementary material online, *Figure S2D*). At the end of three weeks of AngII infusion, HR decreased during high activity compared to saline-infused mice with no differences in activity levels between groups (see Supplementary material online, *Figure S2E and F*). Furthermore, heart rate variability (HRV; a surrogate measure of ANS activity), as assessed by the standard deviation of RR-intervals (SDNN) and root mean squared of the successive differences in RR-interval (RMSSD), was reduced during low and high activity in AngII-infused mice (see Supplementary material online, *Figure S2G and H*).

To directly assess HR responses to β-AR stimulation, mice were acutely injected with the β-AR agonist isoproterenol (ISO; 10 mg/kg). ISO rapidly increased HR in both saline- and AngII-infused mice (*Figure 1A and B*); however, peak HR responses to ISO were smaller in AngII-infused mice compared to saline-infused controls (*Figure 1C and D*). Collectively, these data demonstrate that AngII-infused mice exhibit SAN dysfunction and an impaired ability to increase HR in response to sympathetic nervous system activation and β-AR stimulation.

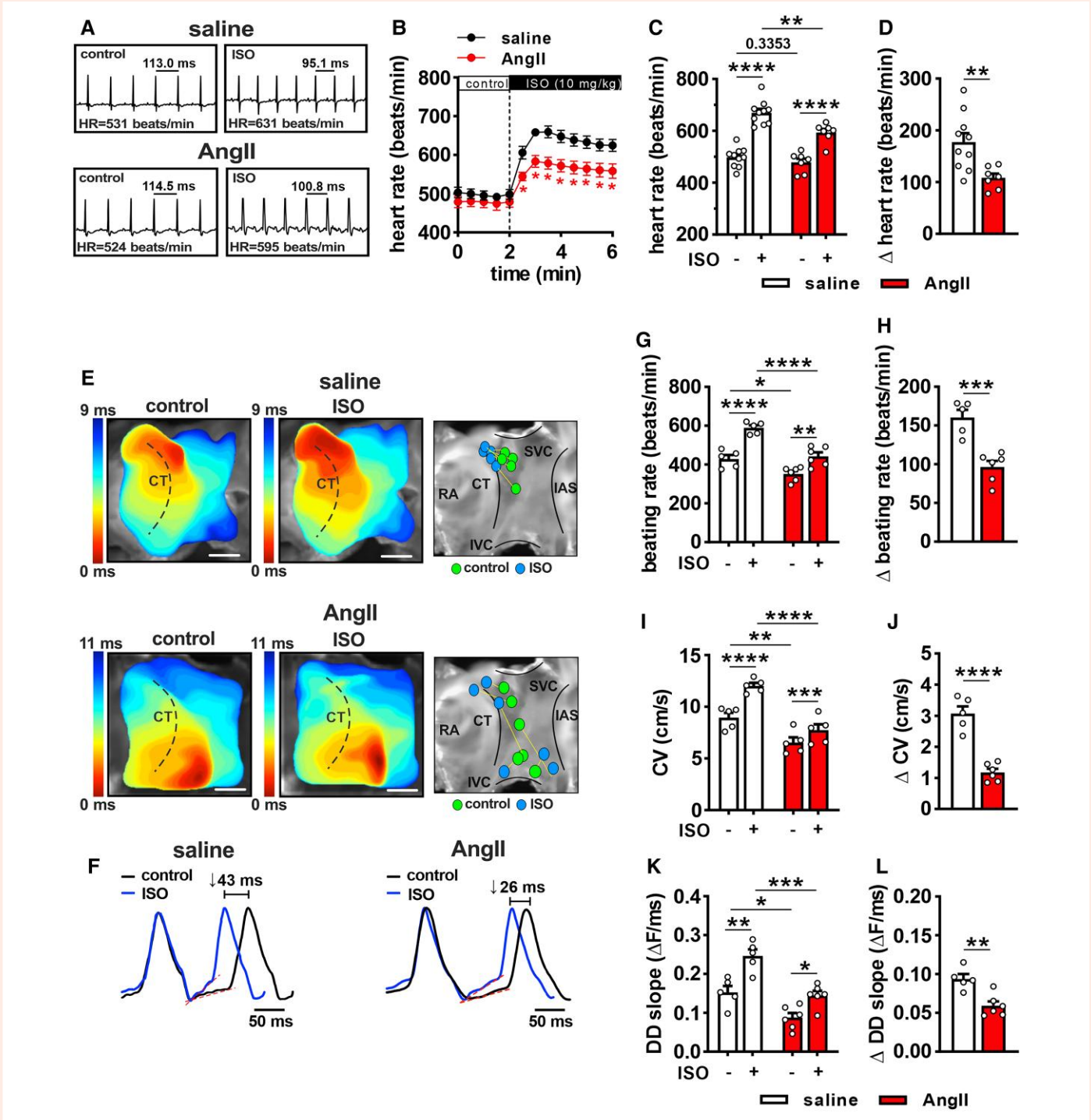

Figure 1 Chronotropic incompetence and impaired SAN electrical conduction in mice with AngII-induced hypertensive heart disease. (*A*) Representative ECG recordings in anaesthetized saline- and AngII-infused mice in control conditions and following acute intraperitoneal injection of isoproterenol (ISO; 10 mg/kg). (*B–D*) Summary of HR over time following ISO injection (*B*), average resting and peak HR responses to ISO (*C*) and change (Δ) in HR after ISO injection (*D*) in anaesthetized saline ($n = 10$) and AngII-infused ($n = 7$) mice. Data in panels *B* and *C* analysed by two-way repeated measures ANOVA with Holm-Sidak *post hoc* test. Data in panel *D* analysed by Student's *t*-test. (*E*) Representative activation maps and initial activation sites in isolated atrial preparations from saline- and AngII-infused mice in control condition and after superfusion of ISO (10 nM). Dashed lines indicate the crista terminalis (CT). Scale bar = 2 mm. RA, right atrium; SVC, superior vena cava; IVC, inferior vena cava; IAS, interatrial septum. (*F*) Optical action potentials (OAPs) from the SAN region of the right atrial posterior wall for saline- and AngII-infused mice before and after ISO. Red lines represent linear fitting of diastolic depolarization (DD) slope. (*G–L*) Summary data and Δ values for atrial preparation beating rate (G and *H*), conduction velocity (CV; *I* and *J*), and OAP DD slope (*K* and *L*) from saline ($n = 5$) and AngII ($n = 6$) atrial preparations before and after application of ISO. Data in panels *G*, *I*, and *K* analysed by two-way repeated measures ANOVA with Holm-Sidak *post hoc* test. Data in panels *H*, *J*, and *L* analysed by Student's *t*-test.

3.2 SAN electrical conduction and β-AR responsiveness are impaired in AngII-infused hearts

To investigate the basis for impaired HR responses to β-AR stimulation in AngII-infused mice, SAN electrical activation and conduction responses to ISO were investigated using high-resolution optical mapping in isolated atrial preparations. Activation maps of the right atrial posterior wall adjacent to the crista terminalis (*Figure 1E*) were used to quantify the location of the initial activation site within the SAN as well as local conduction velocity (CV) in control conditions and after application of ISO (10 nM). As expected, ISO shifted the initial activation site superiorly in saline hearts[29,30] (*Figure 1E*). In contrast, initial activation sites were highly variable in control conditions and displayed irregular shifts in the presence of ISO in AngII-infused hearts (*Figure 1E*). Furthermore, there was an increase in the occurrence of abnormal rhythms such as sinus pauses and rapid ectopic firing in atrial preparations from AngII-infused mice after ISO infusion (see Supplementary material online, *Figure S3*).

Optical APs recorded from the SAN region of the right atrial posterior wall show that the diastolic period between successive APs shortened in response to ISO but this effect was smaller in hearts from AngII-infused mice (*Figure 1F*). Consistent with this, as well as the reduced intrinsic rate and impaired β-AR responsiveness seen *in vivo*, atrial preparations from AngII-infused mice demonstrated lower intrinsic beating rates and reduced responsiveness to ISO compared to saline-infused controls (*Figure 1G* and *H*).

Local CV in the SAN region of the right atrial posterior wall was lower in AngII-infused mice compared to saline-infused mice in control conditions (*Figure 1I*). ISO increased CV in both groups; however, AngII-infused mice had diminished responses to ISO compared to saline-infused controls (*Figure 1I* and *J*). Optical action potentials (OAPs) were also analysed to quantify changes in DD slope in control conditions and in response to ISO (*Figure 1K* and *L*). In control conditions, DD slope was reduced in AngII-infused mice (*Figure 1K*). ISO increased DD slope in both groups; however, these effects were smaller in AngII-infused hearts (*Figure 1L*).

3.3 AngII impairs β-AR regulation of SAN myocyte electrophysiology

To further assess the mechanisms for β-AR desensitization in the SAN of AngII-infused mice, the effects of ISO on spontaneous APs in isolated SAN myocytes were measured (*Figure 2*). Consistent with the reduced intrinsic rates and decreased β-AR responsiveness observed *in vivo* and in isolated atrial preparations, isolated SAN myocytes from AngII-infused mice had reductions in spontaneous AP firing frequency and DD slope in basal conditions as well as smaller increases in AP firing frequency and DD slope after application of ISO (10 nM; *Figure 2A–E*). ISO increased action potential duration at 50% repolarization (APD_{50}) in SAN myocytes from saline- and AngII-infused mice to a similar extent (see Supplementary material online, *Table S2*). There were no differences in maximum diastolic potential or any other measurements of SAN AP morphology between treatment groups in control conditions or in response to ISO (see Supplementary material online, *Table S2*).

I_f and $I_{Ca,L}$ are each importantly involved in mediating β-AR dependent increases in DD slope and HR.[6] Accordingly, the effects of ISO (10 nM) on I_f and $I_{Ca,L}$ were measured in isolated SAN myocytes from saline- and AngII-infused mice. I_f density was reduced in control conditions and after application of ISO in AngII-infused mice (*Figure 2F–H*). While ISO increased I_f density in both groups, the increase in I_f density was smaller in SAN myocytes from AngII-infused mice (*Figure 2H*, Supplementary material online, *Figure S4*). Analysis of I_f steady-state activation kinetics shows that the voltage for 50% channel activation ($V_{1/2(act)}$) was not different between groups in control conditions; however, ISO induced a smaller shift in $V_{1/2(act)}$ in SAN myocytes from AngII-infused mice compared to saline-infused controls (*Figure 2I* and *J*, Supplementary material online, *Figure S4*, Supplementary material online, *Table S3*). No differences were observed in the slope factor for I_f activation at baseline or in response to ISO (see Supplementary material online, *Table S3*).

There were no differences in SAN $I_{Ca,L}$ density at baseline between saline- and AngII-infused mice (*Figure 2K* and *L*). ISO (10 nM) increased $I_{Ca,L}$ density in both groups; however, the magnitude of the increase was smaller in SAN myocytes from AngII-infused mice (*Figure 2M*, Supplementary material online, *Figure S5*). Analysis of $I_{Ca,L}$ steady-state activation kinetics showed that maximum conductance (G_{max}), $V_{1/2(act)}$, and $I_{Ca,L}$ slope factor were not different at baseline between saline- and AngII-infused mice (*Figure 2N*, Supplementary material online, *Figure S5*, Supplementary material online, *Table S4*). In response to ISO, AngII-infused mice had smaller increases in $I_{Ca,L}$, G_{max}, and $V_{1/2(act)}$ compared to saline-infused controls (*Figure 2N* and *O*, Supplementary material online, *Table S4*). There were no differences in the slope factor for $I_{Ca,L}$ activation between saline- and AngII-infused mice after application of ISO (see Supplementary material online, *Table S4*).

Consistent with AP data, CaT frequency was lower in SAN myocytes from AngII-infused mice in control conditions (see Supplementary material online, *Figure S6*). Application of ISO increased CaT frequency in SAN myocytes from saline- and AngII-infused mice, but the increase was smaller in AngII SAN myocytes (see Supplementary material online, *Figure S6*). There were no differences in SAN myocyte CaT amplitude or decay times in control conditions between saline- and AngII-infused mice (see Supplementary material online, *Figure S6*). ISO (10 nM) increased CaT amplitude (see Supplementary material online, *Figure S6A–C*) and shortened CaT decay times; however, these responses to ISO were reduced in AngII SAN myocytes compared to saline controls (see Supplementary material online, *Figure S6*).

3.4 PDE4D desensitizes β-ARs in the SAN in AngII-infused mice

Impaired β-AR signalling could occur due to down-regulation of β-ARs in SAN myocytes or disruption of downstream cAMP signalling.[13,31] There were no differences in protein levels of β_1- and β_2-ARs in the SAN between saline- and AngII-infused hearts (see Supplementary material online, *Figure S7A and B*). Despite this, ISO (10 nM) induced smaller increases in intracellular cAMP in SAN myocytes from AngII-infused mice (*Figure 3A*). PDE4D is a major regulator of cAMP production following β-AR activation in murine hearts.[32] Whole cell SAN PDE4D levels were not different between groups (*Figure 3B* and *C*); however, phosphorylated PDE4D was elevated in the SAN of AngII-infused mice (*Figure 3D*). Consistent with this, there was an increase in whole cell PDE4 activity in the SAN of AngII-infused mice (*Figure 3E*).

Immunocytochemistry was used to determine the co-localization of PDE4D with β-ARs in SAN myocytes from saline- and AngII-infused mice (*Figure 3F* and *G*). These data demonstrate that the co-localization of PDE4D with β_1- and β_2-ARs was increased in AngII SAN myocytes (*Figure 3H* and *I*). Co-immunoprecipitation of β_1- and β_2-ARs with PDE4D also demonstrated increased PDE4D localization surrounding both β-ARs in the SAN of AngII-infused mice (*Figure 3J* and *K*). There were no differences in the mRNA expression of any of the major cardiac PDE4 isoforms in the SAN after AngII infusion (see Supplementary material online, *Figure S7C*).

3.5 PDE4D knockdown increases SAN β-AR responsiveness in AngII-infused hearts

To investigate the role of PDE4D in regulating β-AR signalling in the SAN, mice were injected retro-orbitally with an AAV9 carrying an shRNA for the murine PDE4D isoform (or scrambled control) (*Figure 4A*). Five weeks after AAV9 injection at 1.5×10^{11} genomic copies/mouse, robust infection of the right atrial posterior wall was observed (see Supplementary material online, *Figure S8*), which resulted in a ~65% knockdown of PDE4D in SAN tissue (*Figure 4B* and *C*).

First, the effects of PDE4D knockdown (PDE4D KD) were investigated in normal mice. There were no differences in HR in anaesthetized mice in

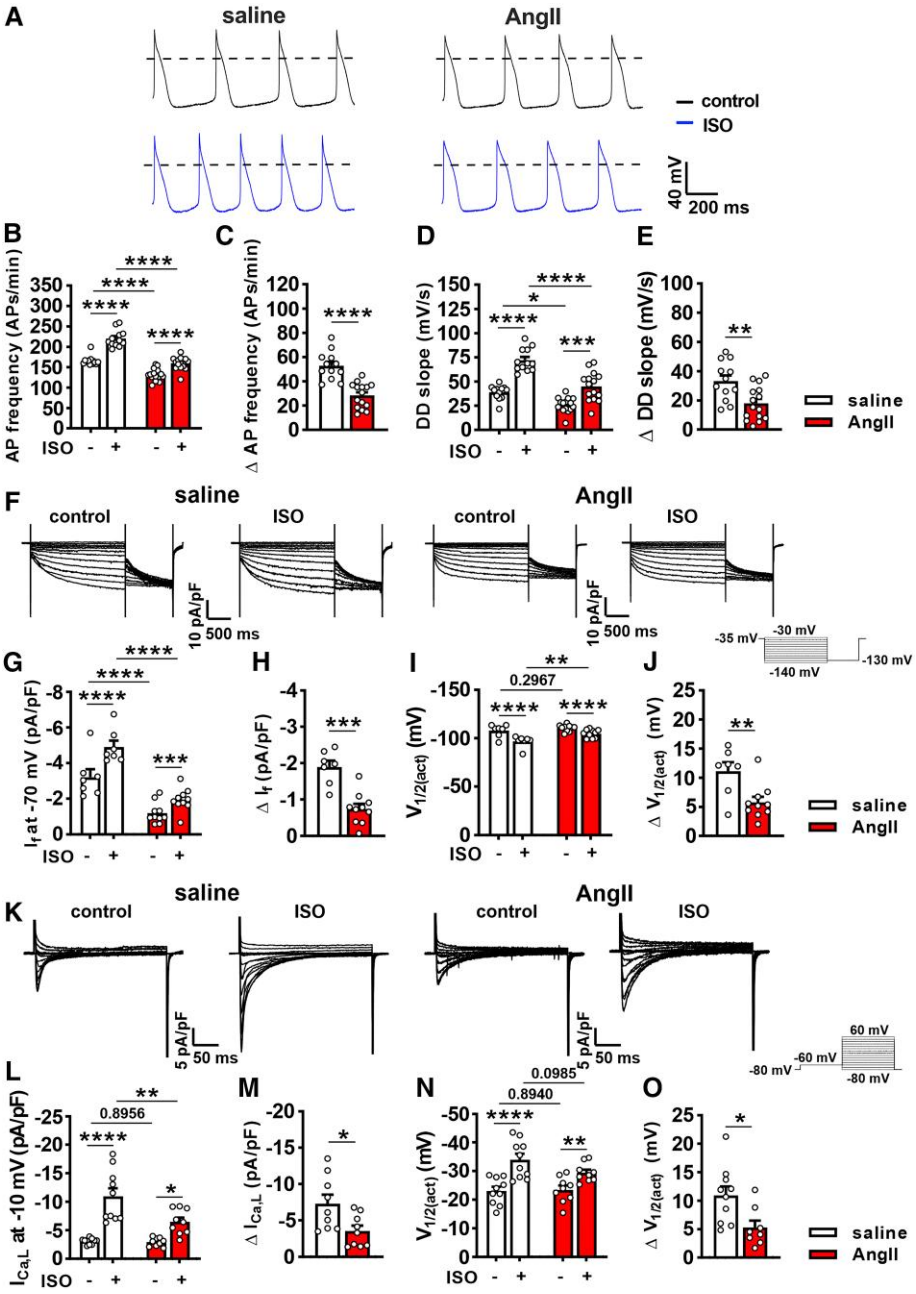

Figure 2 Effects of β-AR stimulation on SAN myocyte electrophysiology in AngII-infused mice. (*A*) Representative spontaneous APs in isolated SAN myocytes from saline- and AngII-infused mice in control conditions and after superfusion of ISO (10 nM). Scale bars apply to all recordings. (*B* and *C*) Summary of AP firing frequency in control conditions and after application of ISO (*B*) and the change in AP firing frequency after ISO (*C*). (*D* and *E*) Summary of SAN myocyte DD slope in control conditions and after application of ISO (*D*) and the change in DD slope after application of ISO (*E*). $n = 12$ cells from four mice for saline and 15 cells from five mice for AngII. See Supplementary material online, *Table S2* for additional AP morphology parameters. (*F*) Representative I_f recordings in isolated SAN myocytes from saline- and AngII-infused mice in control conditions and after superfusion of ISO (10 nM). Voltage clamp protocol shown to the right of the recordings. (*G* and *H*) I_f density at −70 mV in control conditions and after application of ISO (*G*) and the change in I_f density after application of ISO (*H*). (*I* and *J*) I_f $V_{1/2(act)}$ in control conditions and after application of ISO (*I*) and the change in I_f $V_{1/2(act)}$ after application of ISO (*J*). $n = 7$ cells from four mice for saline and 10 cells from seven mice for AngII. Full I_f IV curves and steady-state activation curves are provided in Supplementary material online, *Figure S4*. Refer to Supplementary material online, *Table S3* for additional I_f analysis. (*K*) Representative $I_{Ca,L}$ recordings in isolated SAN myocytes from saline- and AngII-infused mice in control conditions and after superfusion of ISO (10 nM). Voltage clamp protocol shown to the right of the recordings. (*L* and *M*) $I_{Ca,L}$ density at −10 mV in control conditions and after application of ISO (*L*) and the change in $I_{Ca,L}$ density after application of ISO (*M*). (*N* and *O*) $I_{Ca,L}$ $V_{1/2(act)}$ in control conditions and after application of ISO (*N*) and the change in $I_{Ca,L}$ $V_{1/2(act)}$ after application of ISO (*O*). $n = 9$ cells from four mice for saline and 8 cells from five mice for AngII. Full $I_{Ca,L}$ IV curves and steady-state activation curves are provided in Supplementary material online, *Figure S5*. Refer to Supplementary material online, *Table S4* for additional $I_{Ca,L}$ analysis. Panels *B*, *D*, *G*, *I*, *L*, and *N* analysed by two-way repeated measures ANOVA with Holm-Sidak *post hoc* test. Panels *C*, *E*, *H*, *J*, *M*, and *O* analysed by Student's *t*-test.

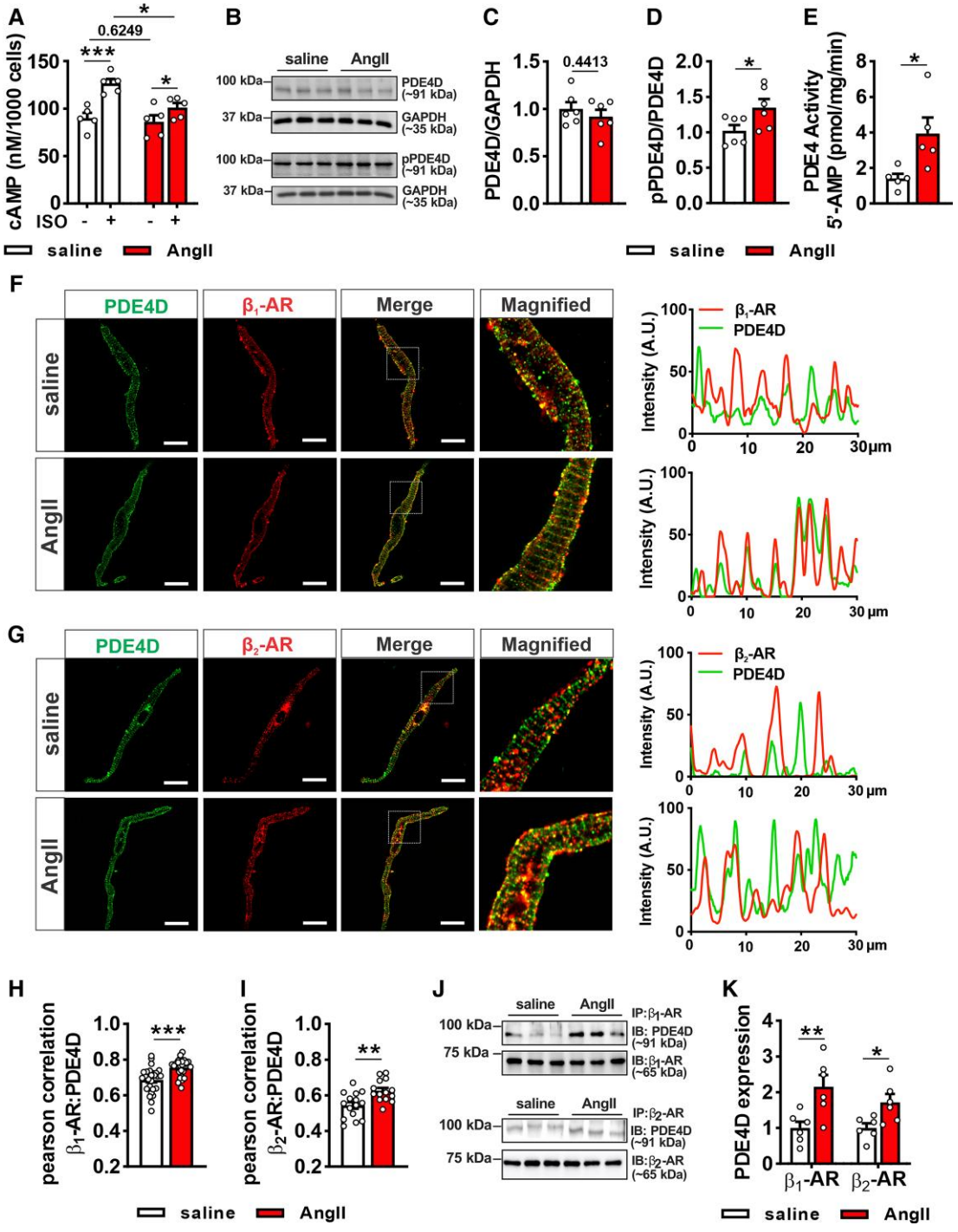

Figure 3 Increased PDE4D activity and localization with β-ARs in the SAN in AngII-infused mice. (*A*) Summary of cAMP levels before and after application of ISO (10 nM) in SAN myocytes from saline ($n = 5$ pooled SAN) and AngII ($n = 5$ pooled SAN) infused mice. Data analysed by two-way ANOVA with Holm-Sidak *post hoc* test. (*B–D*) Representative whole cell lysate western blots (*B*) and summary of protein expression of PDE4D (*C*) and phosphorylated PDE4D (*D*) in the SAN in saline ($n = 6$ pooled SAN) and AngII-infused ($n = 6$ pooled SAN) mice. Data analysed by Student's *t*-test. (*E*) Whole cell lysate PDE4 activity in the SAN of saline ($n = 5$ pooled SAN) and AngII-infused ($n = 5$ pooled SAN) mice. Data analysed by Student's *t*-test. (*F* and *G*) Immunocytochemistry showing fluorescent images of PDE4D, β_1-AR (*F*), and β_2-AR (*G*) and merged images in SAN myocytes from saline- and AngII-infused mice. Boxes in the merged images are shown in the magnified views. Representative intensity plots illustrate overlap of PDE4D with β_1-ARs and β_2-ARs in SAN myocytes from saline- and AngII-infused mice. (*H* and *I*) Pearson correlations of overlap of PDE4D with β_1-ARs (*H*; $n = 26$ myocytes from three saline mice and 25 myocytes from three AngII mice) and β_2-ARs (*I*; $n = 15$ myocytes from three saline mice and 14 myocytes from three AngII mice). Data analysed by Student's *t*-test. (*J* and *K*) Representative β_1- and β_2-AR co-immunoprecipitation western blots (*F*) and summary of PDE4D expression surrounding β_1- and β_2-ARs in the SAN of saline ($n = 6$ pooled SAN) and AngII-infused ($n = 6$ pooled SAN) mice (*G*). Data analysed by two-way ANOVA with Holm-Sidak *post hoc* test. Uncropped western blots are provided in Supplementary material online, *Figure S15*.

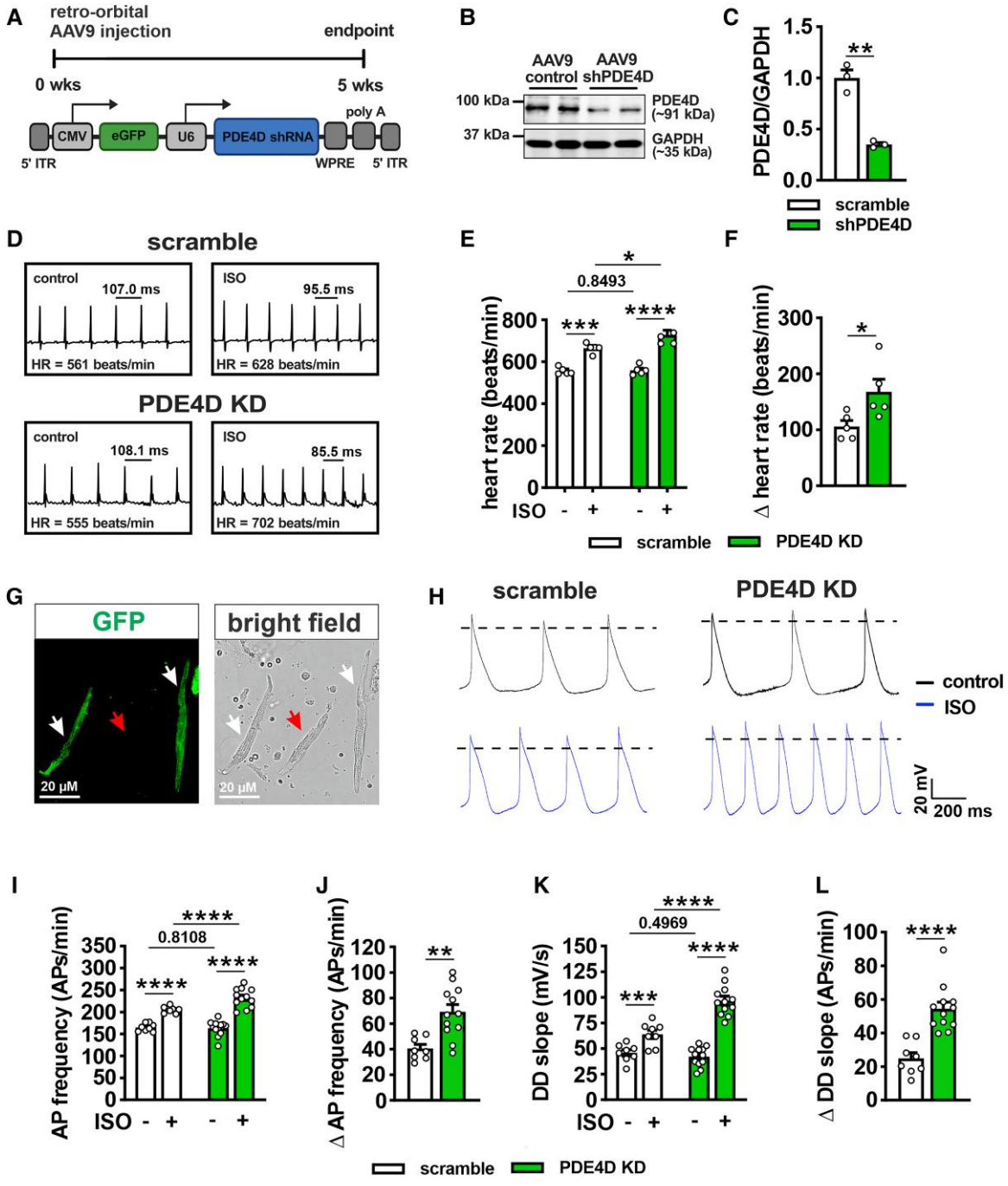

Figure 4 PDE4D knockdown regulates β-AR signalling in the SAN. (*A*) Schematic of AAV9 PDE4D shRNA. (*B* and *C*) PDE4D protein levels in the SAN 5 weeks after injection of mice with a scrambled shRNA (AAV9-control; $n = 3$) and the PDE4D shRNA (AAV9-shPDE4D; $n = 3$). Data analysed by Student's *t*-test. Uncropped western blots are provided in Supplementary material online, *Figure S15*. (*D*) Representative ECGs in anaesthetized PDE4D knockdown (PDE4D KD) mice and scramble controls in control conditions and following acute intraperitoneal injection of ISO (10 mg/kg). (*E* and *F*) Summary of HR in control conditions and after injection of ISO (*E*) and change in HR in response to ISO (*F*) in PDE4D KD mice ($n = 5$) and scramble controls ($n = 5$). Data in panel *E* analysed by two-way ANOVA with Holm-Sidak *post hoc* test. Data in panel *F* analysed by Student's *t*-test. (*G*) Representative image showing AAV9 infected SAN myocytes (GFP^+; white arrows) and non-infected myocytes (red arrow). Only GFP^+ myocytes were used in patch-clamp experiments. (*H*) Spontaneous APs in isolated SAN myocytes from PDE4D KD and scramble control mice in control conditions and after superfusion of ISO (10 nM). Scale bars apply to all recordings. (*I* and *J*) AP firing frequency in control conditions and after application of ISO (*I*) and change in AP firing frequency after application of ISO (*J*). (*K* and *L*) DD slope in control conditions and after application of ISO (*K*) and change in DD slope after application of ISO (*L*). Refer to Supplementary material online, *Table S5* for additional AP analysis. $n = 8$ myocytes from three mice from scramble and 12 myocytes from three mice for PDE4D KD. Data in panels *I* and *K* analysed by two-way repeated measures ANOVA with Holm-Sidak *post hoc* test. Data in panels *J* and *L* analysed by Student's *t*-test.

control conditions between PDE4D KD and scrambled controls; however, acute application of ISO (10 mg/kg) resulted in larger increases in HR in PDE4D KD mice compared to a scrambled shRNA (*Figure 4D–F*). Next, SAN myocytes were isolated from PDE4D KD and scramble control mice, and GFP positive cells were used to assess SAN AP morphology and β-AR sensitivity (*Figure 4G*). Spontaneous AP recordings in these GFP^+ SAN myocytes demonstrate that AP frequency was comparable in control conditions; however, ISO induced larger increases in AP firing frequency after PDE4D KD (*Figures 4I* and *J*). Similarly, DD slope was comparable in control conditions, but increased to a greater extent after ISO application in PDE4D KD myocytes (*Figure 4K* and *L*). Additional AP parameters are provided in Supplementary material online, *Table S5*.

Next, the role of PDE4D in the SAN was investigated in PDE4D knockdown mice infused with AngII. The effects of an acute injection of ISO (10 mg/kg) on HR were measured in saline, AngII-scramble, and AngII-PDE4D knockdown (AngII-PDE4D KD) mice. As expected, AngII-scramble mice had smaller increases in HR following ISO injection (*Figure 5A–C*). In contrast, AngII-PDE4D KD mice showed substantially improved ISO-induced increases in HR that were similar to saline controls (*Figure 5B* and *C*).

Hearts from the same mice used for these *in vivo* experiments were subsequently isolated and used for optical mapping studies. Activation maps and OAPs from the SAN region of the right atrial posterior wall (*Figure 5D*) were used to assess SAN electrical activation and conduction in response to β-AR stimulation. Consistent with the improvements in β-AR signalling observed *in vivo*, isolated atrial preparations from AngII-PDE4D KD mice had improved beating rate responses to ISO compared to AngII-scramble controls (*Figure 5E* and *F*). Furthermore, AngII-PDE4D-KD mice had improved effects of ISO on CV (*Figure 5G* and *H*) as well as larger increases in DD slope compared to AngII-scramble mice (*Figure 5I* and *J*). While SAN chronotropic responses to β-AR stimulation were largely normalized in atrial preparations from AngII-PDE4D-KD mice, initial activation sites in the SAN still exhibited substantial heterogeneity in control conditions compared to saline hearts. Nevertheless, the majority of activation sites still shifted superiorly in response to ISO in PDE4D KD mice (see Supplementary material online, *Figure S9*).

3.6 PDE4D knockdown enhances β-AR signalling in SAN myocytes from AngII-infused mice

The effects of PDE4D knockdown on β-AR responsiveness in isolated GFP^+ SAN myocytes were also measured (*Figure 6*). SAN myocytes from AngII-PDE4D KD mice exhibited increased AP firing frequency and DD slope responses to ISO (10 nM) that were larger than those observed in AngII-scramble SAN myocytes and comparable to SAN myocytes from saline mice (*Figure 6A–E*, Supplementary material online, *Table S6*). While the magnitude of the responses to ISO were normalized, peak AP firing frequency and DD slope were still lower in AngII-PDE4D-KD mice compared to SAN myocytes from saline mice (see Supplementary material online, *Table S6*), likely due to the presence of intrinsic SAN dysfunction due to HCN4 down-regulation.[24] There were no differences in other measurements of SAN AP morphology between treatment groups in control conditions or in response to ISO (see Supplementary material online, *Table S6*).

I_f density was still reduced in AngII-PDE4D KD SAN myocytes to similar levels as AngII-scramble SAN myocytes in control conditions; however, SAN myocytes from AngII-PDE4D KD mice had larger increases in I_f density following ISO (10 nM) application that were similar in magnitude to saline controls (*Figure 7A–C*, Supplementary material online, *Figure S10*). Analysis of I_f activation kinetics showed that ISO induced comparable shifts in $V_{1/2(act)}$ in saline- and AngII-PDE4D KD SAN myocytes (*Figure 7D* and *E*, Supplementary material online, *Figure S10*, Supplementary material online, *Table S7*). No differences in the slope factor for I_f activation were seen at baseline or in response to ISO between any groups (see Supplementary material online, *Table S7*).

SAN $I_{Ca,L}$ density showed no differences at baseline between saline, AngII-scramble, or AngII-PDE4D-KD SAN myocytes (*Figure 7F* and *G*). ISO (10 nM) increased $I_{Ca,L}$ density in all groups; however, SAN myocytes from AngII-scramble mice had smaller increases in $I_{Ca,L}$ density compared to saline mice while SAN myocytes from AngII-PDE4D KD mice had increases in $I_{Ca,L}$ density that were comparable to saline controls (*Figure 7G* and *H*, Supplementary material online, *Figure S11*). Analysis of $I_{Ca,L}$ activation kinetics showed that G_{max}, $V_{1/2(act)}$, and slope factor were not different at baseline between groups (*Figure 7I*, Supplementary material online, *Figure S11*, Supplementary material online, *Table S8*). In response to ISO, AngII-PDE4D KD SAN myocytes had larger increases in $I_{Ca,L}$ G_{max} and $V_{1/2(act)}$ compared to AngII-scramble SAN myocytes, which were indistinguishable from saline-infused mice (*Figure 7I* and *J*, Supplementary material online, *Figure S11*, Supplementary material online, *Table S8*).

ISO (10 nM) also increased CaT frequency, increased CaT amplitude, and reduced CaT decay times in SAN myocytes from saline, AngII-scramble and AngII-PDE4D KD (see Supplementary material online, *Figure S12*). These effects of ISO were impaired in SAN myocytes isolated from AngII-scramble mice compared to saline SAN mice, however, the effects of ISO on CaT morphology were normalized in AngII-PDE4D KD SAN myocytes (see Supplementary material online, *Figure S12*).

To confirm the results of PDE4D knockdown, the effects of the selective PDE4 inhibitor rolipram[11] (Rol; 10 μM) on β-AR responsiveness were measured in isolated SAN myocytes from saline- and AngII-infused mice (see Supplementary material online, *Figure S13*). As expected, ISO increased AP firing frequency in both groups with smaller increases observed in SAN myocytes from AngII-infused mice (see Supplementary material online, *Figure S13A–C*). Addition of Rol in the presence of ISO further increased AP firing frequency in both groups; however, these effects were larger in SAN myocytes from AngII-infused mice (see Supplementary material online, *Figure S13C* and *D*). Similarly, Rol enhanced ISO-induced increases in DD slope in both saline- and AngII-infused mice (see Supplementary material online, *Figure S13E–G*) and normalized the increase in DD slope in SAN myocytes from AngII-infused mice (see Supplementary material online, *Figure S13F* and *G*). Consistent with these improvements in AP firing frequency and DD slope, Rol also produced larger increases in I_f (see Supplementary material online, *Figure S13H–J*) and $I_{Ca,L}$ (see Supplementary material online, *Figure S13K–M*) in ISO-stimulated SAN myocytes from AngII-infused mice compared to saline controls.

PDE3A is also an important regulator of SAN function; therefore, the effects of the selective PDE3 inhibitor milrinone (Mil; 10 μM) on AP morphology were measured in SAN myocytes from saline- and AngII-infused mice (see Supplementary material online, *Figure S14*). Sequential application of ISO (10 nM), and then Mil in the presence of ISO, caused similar increases in AP firing frequency and DD slope in SAN myocytes from saline- and AngII-infused mice (see Supplementary material online, *Figure S14A–E*). AP firing frequency and DD slope remained reduced in AngII-infused SAN myocytes after application of ISO and Mil. Consistent with this, there were no differences in *pde3a* mRNA expression or PDE3A protein levels in the SAN between saline- and AngII-infused mice (see Supplementary material online, *Figure S14F–H*).

4. Discussion

Appropriate HR regulation by the sympathetic nervous system is critical for proper maintenance of cardiac function. In diseases such as hypertensive heart disease and heart failure, HR regulation becomes impaired due to progressive SAN dysfunction and β-AR desensitization.[7,21] Nevertheless, the mechanisms for impaired β-AR regulation of HR in these settings have been poorly understood. In the present study, we used a multi-level approach to assess β-AR regulation of HR and SAN function in mice with AngII-induced hypertensive heart disease. Our findings demonstrate that impaired HR regulation by β-AR activation in AngII-infused mice is due to increased PDE4 activity and PDE4D co-localization with β-ARs in the

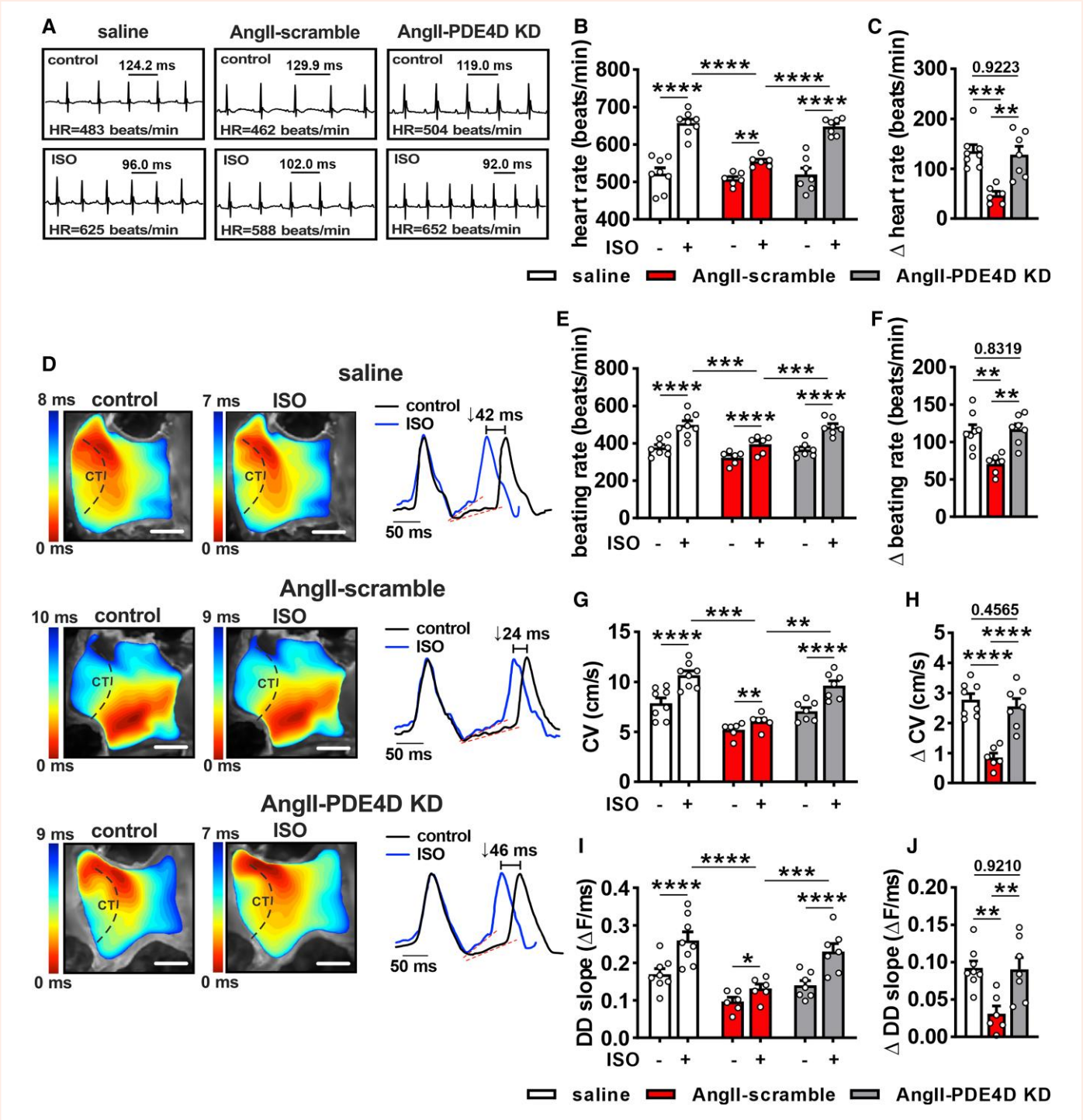

Figure 5 PDE4D knockdown normalizes β-AR responsiveness in AngII-infused mice. (*A–C*) Representative ECGs (*A*), summary of heart rate in control conditions and after intraperitoneal injection of ISO (10 mg/kg; *B*), and change in heart rate after injection of ISO (*C*) for saline ($n = 8$), AngII-scramble ($n = 6$), and AngII-PDE4D KD ($n = 7$) mice. (*D*) Representative activation maps and OAPs in isolated atrial preparations from saline, AngII-scramble, and AngII-PDE4D KD mice in control conditions and after superfusion of ISO (10 nM). Dashed lines indicate the crista terminalis (CT). Scale bar = 2 mm. Red lines on OAPs represent linear fitting of diastolic depolarization (DD) slope. (*E–J*) Summary data in control conditions and after application of ISO as well as Δ values after ISO application for heart rate (*E* and *F*), CV in the SAN region of the right atrial posterior wall (*G* and *H*), and OAP DD slope (*I* and *J*) for saline ($n = 8$), AngII-scramble ($n = 6$), and AngII-PDE4D KD ($n = 7$) mice. Data in panels *B*, *E*, *G*, and *I* analysed by two-way repeated measures ANOVA with Holm-Sidak *post hoc* test. Data in panels *C*, *F*, *H*, and *J* analysed by one-way ANOVA with Holm-Sidak *post hoc* test.

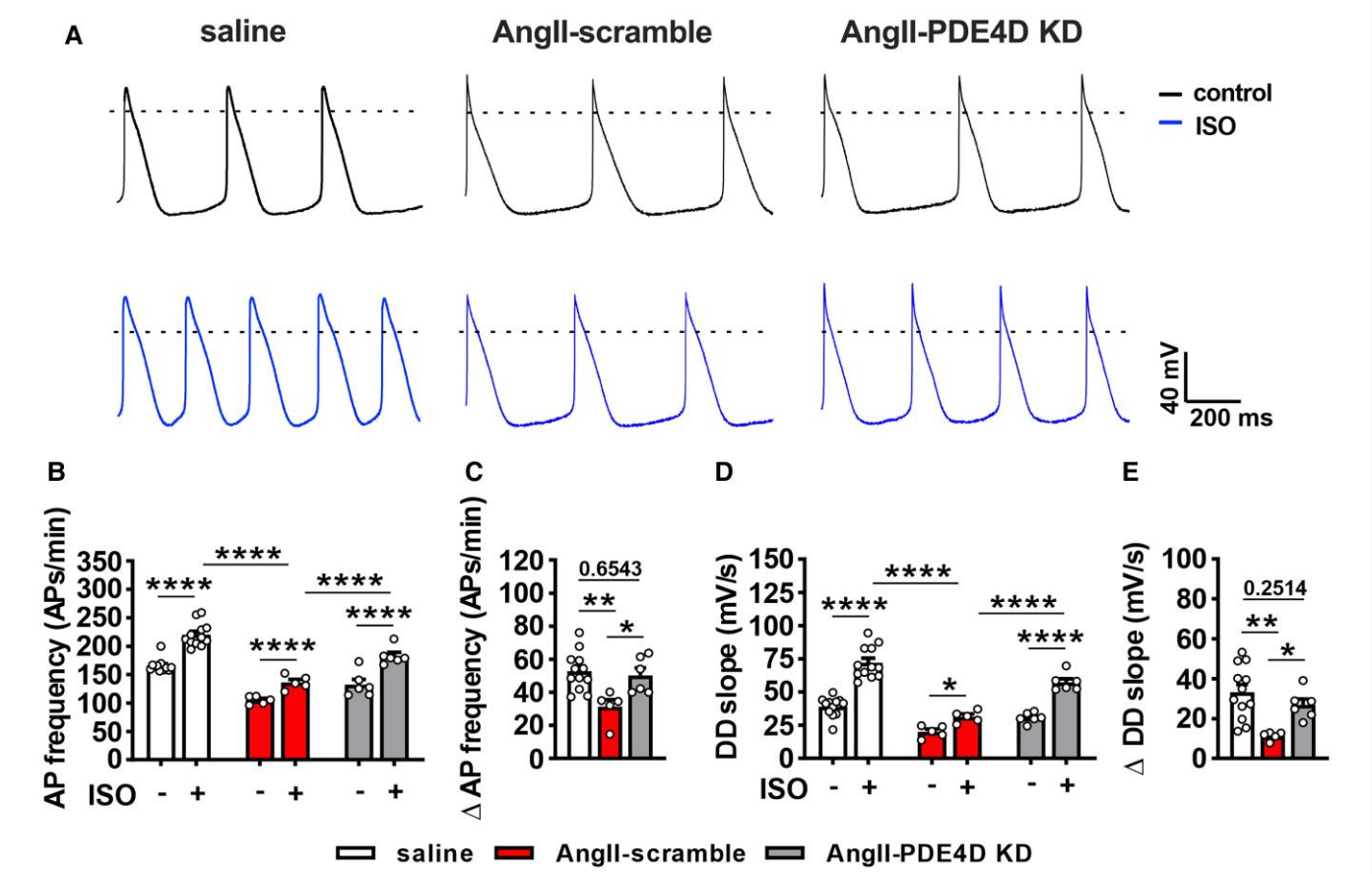

Figure 6 PDE4D knockdown normalizes the effects of isoproterenol on spontaneous AP firing in isolated SAN myocytes from AngII-infused mice. (*A*) Representative spontaneous APs in isolated SAN myocytes from saline, AngII-scramble, and AngII-PDE4D KD mice in control conditions and after superfusion of ISO (10 nM). Scale bars apply to all recordings. (*B* and *C*) AP firing frequency in control conditions and after application of ISO (*B*) and change in AP firing frequency after application of ISO (*C*). (*D* and *E*) DD slope in control conditions and after application of ISO (*D*) and change in DD slope after application of ISO (*E*). Refer to Supplementary material online, *Table S6* for additional AP analysis. $n = 12$ cells from four mice for saline, 5 cells from three mice for AngII-scramble, and 6 cells from three mice for AngII-PDE4D KD. Data in panels *C* and *E* analysed by two-way ANOVA with Holm-Sidak *post hoc* test. Data in panels *D* and *F* analysed by one-way ANOVA with Holm-Sidak *post hoc* test.

SAN, which altered cAMP-dependent regulation of spontaneous AP firing in SAN myocytes. AP firing was impaired due to reduced effects of β-AR agonists on I_f and $I_{Ca,L}$ in SAN myocytes. These findings provide new insight into the mechanisms of chronotropic incompetence in the setting of hypertensive heart disease.

AngII infusion is a well characterized and clinically relevant model of heart disease.[33,34] Hypertension is the number one risk factor for the development of heart failure,[2,35] and these individuals exhibit high levels of circulating plasma AngII.[36] Our present study, as well as our prior work,[24,27,28] shows that AngII-infused mice develop overt cardiac hypertrophy without reductions in ejection fraction or fractional shortening. AngII infusion also caused increases in right and left atrial area, which is an indication of diastolic dysfunction.[37] In conscious mice, AngII infusion resulted in elevated HR during low activity, but lower HR during high activity as well as lower intrinsic HR (i.e. during autonomic blockade), indicating impaired SAN function and increased sympathetic nervous system activity that collectively result in an inability to increase HR in response to increasing activity levels. This is consistent with previous studies demonstrating elevated circulating norepinephrine levels in AngII-infused mice.[23]

Consistent with a chronotropic incompetence phenotype, injection of the β-AR agonist ISO resulted in smaller HR increases in AngII-infused mice. Similar findings in human heart failure with preserved ejection fraction patients show that graded ISO infusions produced smaller increases in HR compared to age-matched controls[21] further supporting the hypothesis that impaired HR regulation is due to impaired β-AR signalling in the SAN. While our model of AngII infusion for three weeks does not induce heart failure with marked systolic dysfunction, our findings suggest that chronotropic incompetence manifests early in the progression from hypertensive heart disease to overt heart failure. Consistent with this, hypertension patients display a higher frequency of chronotropic incompetence compared to normotensive controls.[38] Furthermore, chronotropic incompetence is a powerful predictor of the presence of heart failure symptoms in patients with hypertension.[9]

SAN dysfunction was evident in AngII-infused mice in baseline (control) conditions as indicated by a progressive decline in intrinsic beating rate *in vivo* and in isolated atrial preparations. We have previously demonstrated that intrinsic SAN dysfunction, as well as impairments in conduction and variability in leading activation site, occur in control conditions in AngII mice due to impaired SAN AP firing and fibrosis in the SAN.[23,24] In the present study, we found that in conjunction with intrinsic SAN dysfunction, atrial preparations from AngII-infused mice exhibited smaller increases in beating rate, CV, and DD slope during spontaneous AP firing in response to ISO compared to saline controls. In healthy hearts, β-AR stimulation shifts the leading activation site to a more superior location in the

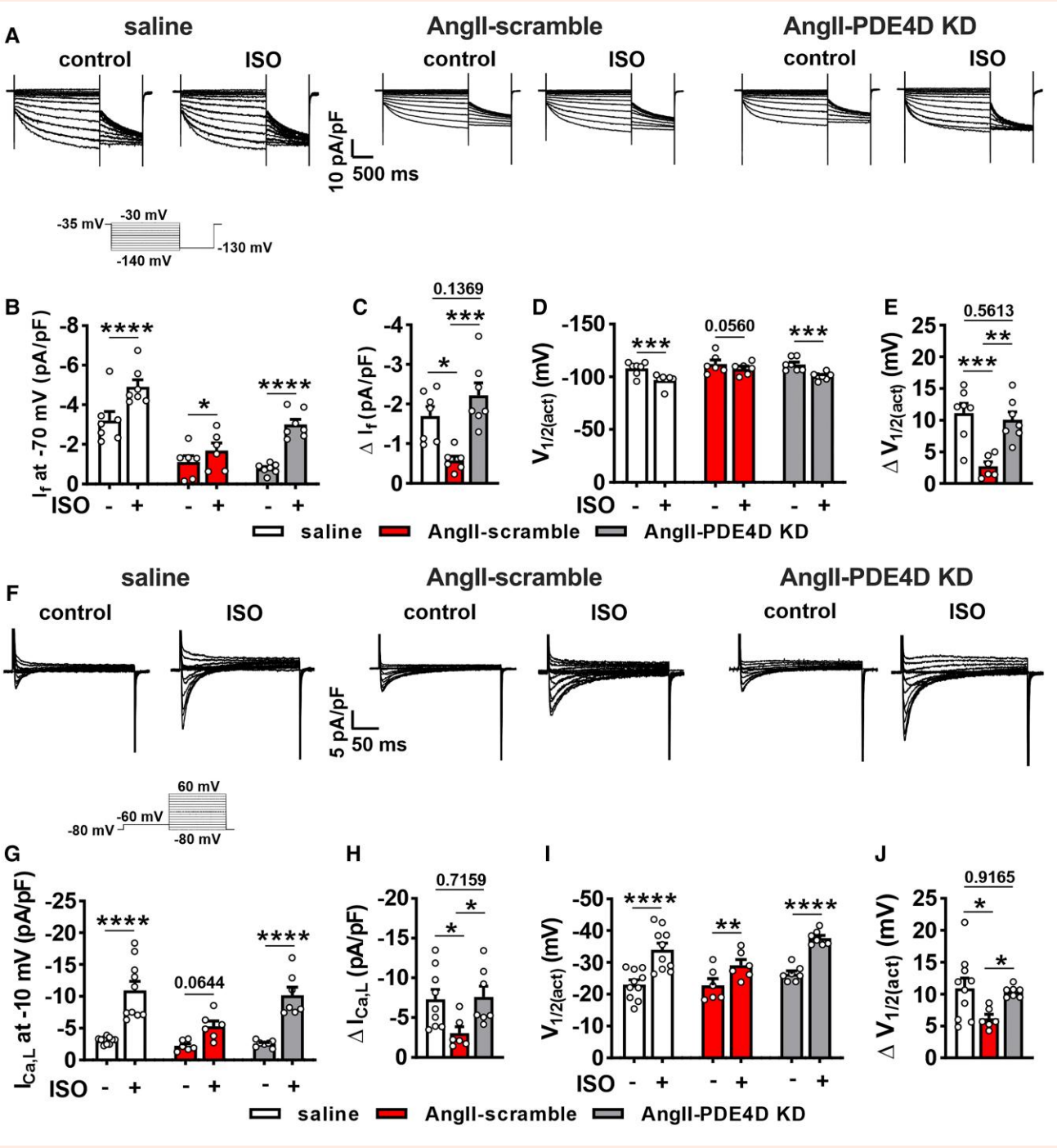

Figure 7 PDE4D knockdown normalizes the effects of ISO on I_f and $I_{Ca,L}$ in isolated SAN myocytes from AngII-infused mice. (*A*) Representative I_f recordings in isolated SAN myocytes from saline, AngII-scramble, and AngII-PDE4D KD mice in control conditions and after superfusion of ISO (10 nM). Scale bars apply to all recordings. Voltage clamp protocol shown below recordings. (*B* and *C*) I_f density at −70 mV in control conditions and after application of ISO (*B*) and change in I_f density after ISO (*C*) in saline, AngII-scramble, and AngII-PDE4D KD SAN myocytes. (*D* and *E*) I_f $V_{1/2(act)}$ in control conditions and after application of ISO (*D*) and change in I_f $V_{1/2(act)}$ after ISO (*E*) in saline, AngII-scramble, and AngII-PDE4D KD SAN myocytes. $n = 7$ cells from four mice for saline, 6 cells from three mice for AngII-scramble, and 7 cells from three mice for AngII-PDE4D KD. Full I_f IV curves and I_f steady-state activation curves are provided in Supplementary material online, *Figure S10*. Refer to Supplementary material online, *Table S7* for additional I_f analysis. (*F*) Representative $I_{Ca,L}$ recordings in isolated SAN myocytes from saline, AngII-scramble, and AngII-PDE4D KD mice in control conditions and after superfusion of ISO (10 nM). Scale bars apply to all recordings. Voltage clamp protocol shown below recordings. (*G–J*) $I_{Ca,L}$ density at −10 mV in control conditions and after application of ISO (*G*) and change in $I_{Ca,L}$ density after ISO (*H*) in saline, AngII-scramble, and AngII-PDE4D KD SAN myocytes. (*I* and *J*) $I_{Ca,L}$ $V_{1/2(act)}$ in control conditions and after application of ISO (*I*) and change in $I_{Ca,L}$ $V_{1/2(act)}$ after ISO (*J*) in saline, AngII-scramble, and AngII-PDE4D KD SAN myocytes. $n = 9$ cells from four mice for saline, 6 cells from three mice for AngII-scramble, and 7 cells from three mice for AngII-PDE4D KD. Full $I_{Ca,L}$ IV curves and $I_{Ca,L}$ steady-state activation curves are provided in Supplementary material online, *Figure S11*. Refer to Supplementary material online, *Table S8* for additional $I_{Ca,L}$ analysis. Data in panels *B*, *D*, *G*, and *I* analysed by two-way repeated measures ANOVA with Holm-Sidak *post hoc* test. Data in panels *C*, *E*, *H*, and *J* analysed by one-way ANOVA with Holm-Sidak *post hoc* test.

SAN[29,30,39] as we observed in saline-infused mice. In contrast, AngII-infused mice had variable changes in initial activation sites following β-AR stimulation and exhibited arrhythmias such as sinus pauses and rapid ectopic activity resembling brady-tachy rhythms commonly seen in individuals with heart disease and SAN dysfunction.[40,41]

Impaired ISO-induced increases in AP firing frequency in isolated SAN myocytes from AngII-infused mice occurred in association with smaller ISO-induced increases I_f and $I_{Ca,L}$ as well as smaller ISO effects on CaT frequency and morphology. ISO increases I_f conductance via the binding of cAMP to HCN channels, negatively shifting the $V_{1/2(act)}$.[5,6,42] ISO also increases $I_{Ca,L}$ density and activation kinetics via cAMP and PKA in SAN myocytes.[6] These effects on I_f and $I_{Ca,L}$ both contribute importantly to the stimulatory effects of ISO on SAN AP frequency.[6,43] SAN myocytes from AngII-infused mice had smaller shifts in $V_{1/2(act)}$ for both I_f and $I_{Ca,L}$ in response to ISO compared to saline controls, which is consistent with reduced cAMP levels in the SAN after AngII infusion.

The impaired effects of ISO on SAN myocyte AP firing also occurred in association with reduced effects on CaT morphology. Local Ca^{2+} releases during the diastolic period, prior to the CaT, also contribute to the generation of the diastolic depolarization, and these processes are cAMP dependent. This creates a 'coupled clock' mechanism for spontaneous AP firing.[5,10] The observation of reduced effects of ISO on membrane currents as well as CaT morphology indicates that multiple cAMP-dependent components that are downstream of the β-ARs, including ion channels and Ca^{2+} regulatory proteins, contribute to chronotropic incompetence in AngII-mediated heart disease.

These findings are consistent with previous studies showing that cAMP generation, assessed by high-resolution FRET-based imaging in SAN myocytes from mice with heart failure, is reduced following β-AR stimulation.[44] Moreover, a recent study in a rat model of heart failure with preserved ejection fraction also demonstrated chronotropic incompetence due to altered SAN electrophysiological responses to β-AR stimulation, although the mechanisms leading to impaired β-AR signalling were not identified in that study.[20] Similar to other studies of SAN dysfunction in heart disease models,[20] we did not observe changes in β-AR expression in the SAN. Conversely, changes in β-AR expression have been well documented in the ventricular myocardium of patients with hypertensive heart disease.[31,45] This indicates that regulation of β-AR expression in the SAN in hypertensive heart disease and heart failure is distinct from the working myocardium.

PDEs are a family of enzymes that critically regulate cyclic nucleotide signalling by compartmentalizing cAMP (and cGMP) signalling cascades.[13,32] PDE4 isoforms are primarily responsible for the degradation of cAMP at high intracellular concentrations such as following β-AR stimulation.[46] Total PDE4 activity, measured using rolipram, was found to be increased in the SAN in AngII-infused mice. Subsequent studies demonstrated increased levels of phosphorylated PDE4D and increased PDE4D co-localization with β_1- and β_2-ARs in the SAN of AngII-infused mice. Enhanced PDE4D recruitment to β-ARs is well defined[16,17,47–49] and can be initiated by multiple neurohumoral factors such as high levels of catecholamine stimulation[49] or even directly by AngII.[16] While this can provide a negative feedback mechanism whereby phosphorylation of PDE4D by PKA or other kinases increases its hydrolytic activity for cAMP and facilitates recruitment to β-ARs to prevent excessive catecholamine signalling,[50] the present study demonstrates that changes in PDE4D activity and localization lead to impaired HR responses and SAN function in AngII-mediated heart disease.

To confirm the role of PDE4D in AngII-mediated β-AR desensitization, we utilized an AAV9-mediated PDE4D knockdown model that produced ~65% knockdown of PDE4D in the SAN. In normal mice, PDE4D KD did not have major effects on basal HR *in vivo* or on SAN AP firing frequency in control conditions. In contrast, ISO elicited much larger increases in HR and SAN AP firing frequency in PDE4D KD mice, which is consistent with a role for PDE4D in regulating cAMP during β-AR stimulation in the SAN.

Critically, PDE4D knockdown largely normalized the magnitude of the effects of ISO on HR, CV, and DD slope in AngII-infused mice to levels that were comparable to saline controls. At a cellular level, this was due to the normalization of the effects of ISO on I_f, $I_{Ca,L}$, and CaT morphology in SAN myocytes. This is consistent with a previous study demonstrating that PDE4D knockout mice have exaggerated atrial cAMP responses to β-AR stimulation.[51] These findings demonstrate that the changes in PDE4D activity and localization identified here can account for the impaired responses to ISO in the SAN in AngII-mediated heart disease. Furthermore, these studies demonstrate that a partial reduction of PDE4D protein levels is sufficient to normalize PDE4D signalling in AngII-mediated hypertensive heart disease.

Our prior studies show that I_f is reduced and that $I_{Ca,L}$ is not different in control conditions (i.e. without ISO) in SAN myocytes from AngII-infused mice.[24] The basal reduction in I_f occurs in association with reduced HCN4 expression rather than a change in I_f steady-state activation kinetics.[24] Our present study is consistent with these prior results and explains why there are no differences in I_f or $I_{Ca,L}$ $V_{1/2(act)}$ in control conditions, including after PDE4D knockdown. This further supports the conclusion that PDE4D primarily controls cAMP during acute β-AR stimulation. We have also previously shown that the leading activation site in the right atrial posterior wall is more variable in AngII-infused mice, which was also seen in the present study. ISO is known to shift the leading activation site towards the superior region of the SAN,[30] which was observed in saline-infused mice in the present study, but less so in AngII-infused mice. Interestingly, after PDE4D knockdown, ISO induced superior shifts in leading activation site in most AngII-infused hearts, although the location of these leading activation sites remained more variable than in saline-infused hearts. The persistent variability, even after PDE4D knockdown, may be because of reductions in HCN4 expression and the presence of fibrosis in the SAN in AngII-infused mice.[24]

Acute application of rolipram, a specific PDE4 family inhibitor, increased SAN responsiveness to β-AR signalling by increasing ISO-stimulated spontaneous AP firing in SAN myocytes from AngII-infused mice. Interestingly, PDE4 inhibitors can augment catecholamine stimulated cAMP levels in human atria[51] but appear to have little inotropic effects in ventricular myocardium.[52] This may be due to differential expression and/or localization of PDE4 isoforms in atrial vs. ventricular myocardium. We have previously shown that in murine hearts, expression of PDE4D is ~two-fold higher in the SAN compared to the ventricles[11] consistent with a prominent role in regulating β-AR signalling in the SAN. Importantly, inhibition of PDE3 with milrinone did not improve ISO-responsiveness in SAN myocytes from AngII-infused mice, further supporting a primary role for PDE4 in chronotropic incompetence.

Some limitations of our study should be noted. In addition to the alterations identified in the present study, other factors may also contribute to chronotropic incompetence. For example, it is possible that compartmentalization of adenylyl cyclases or ion channels or changes in ion channel trafficking may occur. These could be investigated in future studies. While our studies demonstrate changes in SAN CaT morphology after ISO application in AngII-infused mice, a detailed analysis of sarcoplasmic reticulum Ca^{2+} handling and local Ca^{2+} release events during diastolic depolarization was not performed. The present study was conducted in a well-established model of hypertensive heart disease with cardiac hypertrophy. Future studies should investigate the role of PDE4D in the SAN in models of heart failure with preserved or reduced ejection fraction. Future studies could also investigate the impacts of PDE4D overexpression on β-AR function in the SAN in healthy and diseased hearts. From a translational perspective, it is important to recognize that the expression and regulation of PDE isoforms may differ between mice and humans. PDE4D regulation of β-AR function is well conserved between species[53]; however, it will be important to investigate the role of PDE4D in the SAN in human patients with hypertensive heart disease and heart failure in future studies.

5. Conclusion

AngII-induced hypertensive heart disease results in impaired HR responses to β-AR signalling due to up-regulation of PDE4D activity, particularly

around β-ARs in the SAN. Our findings identify new mechanisms for chronotropic incompetence and demonstrate a critical role for PDE4D in regulating SAN β-AR signalling. This may have important implications for understanding and treating SAN dysfunction in the setting of hypertensive heart disease.

Supplementary material

Supplementary material is available at *Cardiovascular Research* online.

Authors' contributions

T.W.D. and R.A.R. contributed to conception and experimental design. T.W.D. performed and analysed all experiments except immunocytochemistry that was performed by M.D.M. and echocardiography that was performed by D.D.B. T.W.D. and R.A.R. prepared the figures and wrote the manuscript. All authors read and approved the final manuscript.

Acknowledgements

The authors thank Dr Hailey Jansen for her assistance with some experiments.

Conflict of interest: None declared.

Funding

This work was supported by the Canadian Institutes of Health Research to R.A.R. (PJT166105 and PJT180474). T.W.D. held a Canadian Institutes of Health Research Doctoral Research Award.

Data availability

The data supporting the findings of this study are available from the corresponding author upon reasonable request.

References

1. Mills KT, Bundy JD, Kelly TN, Reed JE, Kearney PM, Reynolds K, Chen J, He J. Global disparities of hypertension prevalence and control: a systematic analysis of population-based studies from 90 countries. *Circulation* 2016;**134**:441–450.
2. Andersson C, Vasan RS. Epidemiology of heart failure with preserved ejection fraction. *Heart Fail Clin* 2014;**10**:377–388.
3. Ziaeian B, Fonarow GC. Epidemiology and aetiology of heart failure. *Nat Rev Cardiol* 2016;**13**:368–378.
4. Drazner MH. The progression of hypertensive heart disease. *Circulation* 2011;**123**:327–334.
5. MacDonald EA, Rose RA, Quinn TA. Neurohumoral control of sinoatrial node activity and heart rate: insight from experimental models and findings from humans. *Front Physiol* 2020;**11**:170.
6. Mangoni ME, Nargeot J. Genesis and regulation of the heart automaticity. *Physiol Rev* 2008;**88**:919–982.
7. Brubaker PH, Kitzman DW. Chronotropic incompetence: causes, consequences, and management. *Circulation* 2011;**123**:1010–1020.
8. Zweerink A, van der Lingen ACJ, Handoko ML, van Rossum AC, Allaart CP. Chronotropic incompetence in chronic heart failure. *Circ Heart Fail* 2018;**11**:e004969.
9. Borlaug BA, Melenovsky V, Russell SD, Kessler K, Pacak K, Becker LC, Kass DA. Impaired chronotropic and vasodilator reserves limit exercise capacity in patients with heart failure and a preserved ejection fraction. *Circulation* 2006;**114**:2138–2147.
10. Lakatta EG, Maltsev VA, Vinogradova TM. A coupled SYSTEM of intracellular Ca^{2+} clocks and surface membrane voltage clocks controls the timekeeping mechanism of the heart's pacemaker. *Circ Res* 2010;**106**:659–673.
11. Hua R, Adamczyk A, Robbins C, Ray G, Rose RA. Distinct patterns of constitutive phosphodiesterase activity in mouse sinoatrial node and atrial myocardium. *PLoS One* 2012;**7**:e47652.
12. Vinogradova TM, Kobrinsky E, Lakatta EG. Dual activation of phosphodiesterases 3 and 4 regulates basal spontaneous beating rate of cardiac pacemaker cells: role of compartmentalization? *Front Physiol* 2018;**9**:1301.
13. Xiang YK. Compartmentalization of beta-adrenergic signals in cardiomyocytes. *Circ Res* 2011;**109**:231–244.
14. Vinogradova TM, Sirenko S, Lukyanenko YO, Yang D, Tarasov KV, Lyashkov AE, Varghese NJ, Li Y, Chakir K, Ziman B, Lakatta EG. Basal spontaneous firing of rabbit sinoatrial node cells is regulated by dual activation of PDEs (phosphodiesterases) 3 and 4. *Circ Arrhythm Electrophysiol* 2018;**11**:e005896.
15. Richter W, Jin SL, Conti M. Splice variants of the cyclic nucleotide phosphodiesterase PDE4D are differentially expressed and regulated in rat tissue. *Biochem J* 2005;**388**:803–811.
16. Shi Q, Li M, Mika D, Fu Q, Kim S, Phan J, Shen A, Vandecasteele G, Xiang YK. Heterologous desensitization of cardiac beta-adrenergic signal via hormone-induced betaAR/arrestin/PDE4 complexes. *Cardiovasc Res* 2017;**113**:656–670.
17. Richter W, Day P, Agrawal R, Bruss MD, Granier S, Wang YL, Rasmussen SG, Horner K, Wang P, Lei T, Patterson AJ, Kobilka B, Conti M. Signaling from beta1- and beta2-adrenergic receptors is defined by differential interactions with PDE4. *EMBO J* 2008;**27**:384–393.
18. Xiang Y, Naro F, Zoudilova M, Jin SL, Conti M, Kobilka B. Phosphodiesterase 4D is required for beta2 adrenoceptor subtype-specific signaling in cardiac myocytes. *Proc Natl Acad Sci U S A* 2005;**102**:909–914.
19. Zaccolo M, Pozzan T. Discrete microdomains with high concentration of cAMP in stimulated rat neonatal cardiac myocytes. *Science* 2002;**295**:1711–1715.
20. Mesquita T, Zhang R, Cho JH, Zhang R, Lin YN, Sanchez L, Goldhaber JI, Yu JK, Liang JA, Liu W, Trayanova NA, Cingolani E. Mechanisms of sinoatrial node dysfunction in heart failure with preserved ejection fraction. *Circulation* 2022;**145**:45–60.
21. Sarma S, Stoller D, Hendrix J, Howden E, Lawley J, Livingston S, Adams-Huet B, Holmes C, Goldstein DS, Levine BD. Mechanisms of chronotropic incompetence in heart failure with preserved ejection fraction. *Circ Heart Fail* 2020;**13**:e006331.
22. Colucci WS, Ribeiro JP, Rocco MB, Quigg RJ, Creager MA, Marsh JD, Gauthier DF, Hartley LH. Impaired chronotropic response to exercise in patients with congestive heart failure. Role of postsynaptic beta-adrenergic desensitization. *Circulation* 1989;**80**:314–323.
23. Dorey TW, Moghtadaei M, Rose RA. Altered heart rate variability in angiotensin II-mediated hypertension is associated with impaired autonomic nervous system signaling and intrinsic sinoatrial node dysfunction. *Heart Rhythm* 2020;**17**:1360–1370.
24. Mackasey M, Egom EE, Jansen HJ, Hua R, Moghtadaei M, Liu Y, Kaur J, McRae MD, Bogachev O, Rafferty SA, Ray G, Kirkby AW, Rose RA. Natriuretic peptide receptor-C protects against angiotensin II-mediated sinoatrial node disease in mice. *JACC Basic Transl Sci* 2018;**3**:824–843.
25. Dorey TW, Mackasey M, Jansen HJ, McRae MD, Bohne LJ, Liu Y, Belke DD, Atkinson L, Rose RA. Natriuretic peptide receptor B maintains heart rate and sinoatrial node function via cyclic GMP-mediated signalling. *Cardiovasc Res* 2022;**118**:1917–1931.
26. Tuomi JM, Bohne LJ, Dorey TW, Jansen HJ, Liu Y, Jones DL, Rose RA. Distinct effects of ibrutinib and acalabrutinib on mouse atrial and sinoatrial node electrophysiology and arrhythmogenesis. *J Am Heart Assoc* 2021;**10**:e022369.
27. Jansen HJ, Mackasey M, Moghtadaei M, Belke DD, Egom EE, Tuomi JM, Rafferty SA, Kirkby AW, Rose RA. Distinct patterns of atrial electrical and structural remodeling in angiotensin II mediated atrial fibrillation. *J Mol Cell Cardiol* 2018;**124**:12–25.
28. Jansen HJ, Mackasey M, Moghtadaei M, Liu Y, Kaur J, Egom EE, Tuomi JM, Rafferty SA, Kirkby AW, Rose RA. NPR-C (natriuretic peptide receptor-C) modulates the progression of angiotensin II-mediated atrial fibrillation and atrial remodeling in mice. *Circ Arrhythm Electrophysiol* 2019;**12**:e006863.
29. Lang D, Petrov V, Lou Q, Osipov G, Efimov IR. Spatiotemporal control of heart rate in a rabbit heart. *J Electrocardiol* 2011;**44**:626–634.
30. Azer J, Hua R, Krishnaswamy PS, Rose RA. Effects of natriuretic peptides on electrical conduction in the sinoatrial node and atrial myocardium of the heart. *J Physiol* 2014;**592**:1025–1045.
31. Post SR, Hammond HK, Insel PA. Beta-adrenergic receptors and receptor signaling in heart failure. *Annu Rev Pharmacol Toxicol* 1999;**39**:343–360.
32. Bender AT, Beavo JA. Cyclic nucleotide phosphodiesterases: molecular regulation to clinical use. *Pharmacol Rev* 2006;**58**:488–520.
33. Tsukamoto Y, Mano T, Sakata Y, Ohtani T, Takeda Y, Tamaki S, Omori Y, Ikeya Y, Saito Y, Ishii R, Higashimori M, Kaneko M, Miwa T, Yamamoto K, Komuro I. A novel heart failure mice model of hypertensive heart disease by angiotensin II infusion, nephrectomy, and salt loading. *Am J Physiol Heart Circ Physiol* 2013;**305**:H1658–H1667.
34. Crowley SD, Gurley SB, Herrera MJ, Ruiz P, Griffiths R, Kumar AP, Kim HS, Smithies O, Le TH, Coffman TM. Angiotensin II causes hypertension and cardiac hypertrophy through its receptors in the kidney. *Proc Natl Acad Sci U S A* 2006;**103**:17985–17990.
35. Andersen MJ, Borlaug BA. Heart failure with preserved ejection fraction: current understandings and challenges. *Curr Cardiol Rep* 2014;**16**:501.
36. Opie LH, Sack MN. Enhanced angiotensin II activity in heart failure: reevaluation of the counterregulatory hypothesis of receptor subtypes. *Circ Res* 2001;**88**:654–658.
37. Schnelle M, Catibog N, Zhang M, Nabeebaccus AA, Anderson G, Richards DA, Sawyer G, Zhang X, Toischer K, Hasenfuss G, Monaghan MJ, Shah AM. Echocardiographic evaluation of diastolic function in mouse models of heart disease. *J Mol Cell Cardiol* 2018;**114**:20–28.
38. Shin K, Shin K, Hong S. Heart rate recovery and chronotropic incompetence in patients with prehypertension. *Minerva Med* 2015;**106**:87–94.
39. Glukhov AV, Fedorov VV, Anderson ME, Mohler PJ, Efimov IR. Functional anatomy of the murine sinus node: high-resolution optical mapping of ankyrin-B heterozygous mice. *Am J Physiol Heart Circ Physiol* 2010;**299**:H482–H491.
40. Bloch Thomsen PE, Jons C, Raatikainen MJ, Moerch Joergensen R, Hartikainen J, Virtanen V, Boland J, Anttonen O, Gang UJ, Hoest N, Boersma LV, Platou ES, Becker D, Messier MD, Huikuri HV, Cardiac A; Risk Stratification After Acute Myocardial Infarction Study Group. Long-term recording of cardiac arrhythmias with an implantable cardiac monitor in patients with reduced ejection fraction after acute myocardial infarction: the Cardiac Arrhythmias and Risk Stratification After Acute Myocardial Infarction (CARISMA) study. *Circulation* 2010;**122**:1258–1264.
41. John RM, Kumar S. Sinus node and atrial arrhythmias. *Circulation* 2016;**133**:1892–1900.
42. DiFrancesco D. The role of the funny current in pacemaker activity. *Circ Res* 2010;**106**:434–446.

43. Zaza A, Robinson RB, DiFrancesco D. Basal responses of the L-type Ca^{2+} and hyperpolarization-activated currents to autonomic agonists in the rabbit sino-atrial node. *J Physiol* 1996;**491**:347–355.
44. Reddy GR, Ren L, Thai PN, Caldwell JL, Zaccolo M, Bossuyt J, Ripplinger CM, Xiang YK, Nieves-Cintron M, Chiamvimonvat N, Navedo MF. Deciphering cellular signals in adult mouse sinoatrial node cells. *iScience* 2022;**25**:103693.
45. de Lucia C, Eguchi A, Koch WJ. New insights in cardiac beta-adrenergic signaling during heart failure and aging. *Front Pharmacol* 2018;**9**:904.
46. Kokkonen K, Kass DA. Nanodomain regulation of cardiac cyclic nucleotide signaling by phosphodiesterases. *Annu Rev Pharmacol Toxicol* 2017;**57**:455–479.
47. Mika D, Richter W, Conti M. A CaMKII/PDE4D negative feedback regulates cAMP signaling. *Proc Natl Acad Sci U S A* 2015;**112**:2023–2028.
48. Perry SJ, Baillie GS, Kohout TA, McPhee I, Magiera MM, Ang KL, Miller WE, McLean AJ, Conti M, Houslay MD, Lefkowitz RJ. Targeting of cyclic AMP degradation to beta 2-adrenergic receptors by beta-arrestins. *Science* 2002;**298**:834–836.
49. Liu S, Li Y, Kim S, Fu Q, Parikh D, Sridhar B, Shi Q, Zhang X, Guan Y, Chen X, Xiang YK. Phosphodiesterases coordinate cAMP propagation induced by two stimulatory G protein-coupled receptors in hearts. *Proc Natl Acad Sci U S A* 2012;**109**:6578–6583.
50. Eschenhagen T. PDE4 in the human heart—major player or little helper? *Br J Pharmacol* 2013;**169**:524–527.
51. Molina CE, Leroy J, Richter W, Xie M, Scheitrum C, Lee IO, Maack C, Rucker-Martin C, Donzeau-Gouge P, Verde I, Llach A, Hove-Madsen L, Conti M, Vandecasteele G, Fischmeister R. Cyclic adenosine monophosphate phosphodiesterase type 4 protects against atrial arrhythmias. *J Am Coll Cardiol* 2012;**59**:2182–2190.
52. Molenaar P, Christ T, Hussain RI, Engel A, Berk E, Gillette KT, Chen L, Galindo-Tovar A, Krobert KA, Ravens U, Levy FO, Kaumann AJ. PDE3, but not PDE4, reduces beta1- and beta2-adrenoceptor-mediated inotropic and lusitropic effects in failing ventricle from metoprolol-treated patients. *Br J Pharmacol* 2013;**169**:528–538.
53. Richter W, Xie M, Scheitrum C, Krall J, Movsesian MA, Conti M. Conserved expression and functions of PDE4 in rodent and human heart. *Basic Res Cardiol* 2011;**106**:249–262.

Translational perspective

Chronotropic incompetence and impaired β-adrenergic receptor (β-AR) signalling are prevalent in hypertensive heart disease and heart failure leading to poor heart rate control and increased mortality. We report that impaired β-AR responsiveness in the sinoatrial node (SAN) in AngII-mediated hypertensive heart disease occurs due to increased activity of phosphodiesterase 4D (PDE4D) in the SAN. This results in impaired effects of β-AR agonists on SAN spontaneous action potential firing and SAN ionic currents (I_f and $I_{Ca,L}$). These data suggest that PDE4D could be a novel target for treating chronotropic incompetence in hypertensive heart disease.